Energy Storage Materials 1 (2015) 119–126

Contents lists available at ScienceDirect

Energy Storage Materials

journal homepage: www.elsevier.com/locate/ensm

Binder-free activated graphene compact films for all-solid-state micro-supercapacitors with high areal and volumetric capacitances

Zhong-Shuai Wu [a,c], Sheng Yang [a], Lili Zhang [d], Jakob B. Wagner [d], Xinliang Feng [b,*], Klaus Müllen [a,*]

[a] Max-Planck-Institut für Polymerforschung, Ackermannweg 10, 55128 Mainz, Germany
[b] Center for Advancing Electronics Dresden (cfaed) & Department of Chemistry and Food Chemistry, Technische Universität Dresden, 01062 Dresden, Germany
[c] Dalian Institute of Chemical Physics, Chinese Academy of Sciences, Dalian National Laboratory for Clean Energy, Dalian 116023, China
[d] Center for Electron Nanoscopy, Technical University of Denmark, Fysikvej, Bygning 307, 2800 Kongens Lyngby, Denmark

ARTICLE INFO

Article history:
Received 25 July 2015
Received in revised form
14 September 2015
Accepted 14 September 2015
Available online 13 October 2015

ABSTRACT

Micro-supercapacitors (MSCs) hold great promise as highly competitive miniaturized power sources satisfying the increased demand in microelectronics; however, simultaneously achieving high areal and volumetric capacitances is still a great challenge. Here we demonstrated the designed construction of binder-free, electrically conductive, nanoporous activated graphene (AG) compact films for high-performance MSCs. The binder-free AG films are fabricated by alternating deposition of electrochemically exfoliated graphene (EG) and nanoporous AG with a high specific surface area of 2920 m^2/g, and then dry transferring onto the target substrates with a high-pressure mechanical densification process. Remarkably, the resulting compressed AG films showed uniform morphology in lateral dimensions, high conductivity (60 S/cm), nanoporous feature (<10 nm), and high packing density (0.8 g/cm^3). The all-solid-state MSCs (AG-MSCs) based on these AG films simultaneously delivered an unprecedented areal capacitance of 89.5 mF/cm^2 and volumetric capacitance of 147 F/cm^3 for MSCs at 10 mV/s. Moreover, the fabricated AG-MSCs could be operated at a large scan rate of 10,000 mV/s, and showed outstanding cycling stability (capacitance retention of $>99.6\%$ after 10,000 cycles). Our results suggested that AG-MSCs are competitive for prospective applications of miniaturized energy storage devices.

1. Introduction

Micro-supercapacitors (MSCs) hold promise as highly competitive miniaturized power sources satisfying the increased demand in portable, wearable and implantable microelectronics, since they potentially integrate the unprecedented advantages of high power density of electrolytic capacitor (10^2–10^3 W cm^{-3}) and energy delivery of lithium thin-film battery (10 mW h cm^{-3}) [1–4]. The pseudocapacitive MSCs utilizing Faradaic reactions of metal oxides, e.g., RuO_2 [5], MnO_2 [6], VS_2 [7], and conducting polymers, e.g., polypyrrole [8], and polyaniline [9,10], have been intensively explored, but suffer from low power density, short cycle life, and slow frequency response [11]. To overcome these drawbacks, carbon-based MSCs store electric energy in a double layer at electrochemically stable, high specific surface area electrodes have gained increased attentions, including activated carbon [12,13], carbide-derived carbon [14,15], onion-like carbon [16], carbon nanotubes (CNTs) [17,18], nanoporous carbon (NPC) [19], and graphene [2,3,20–23]. In particular, high surface area of nanocarbons for MSCs can provide an extensively accessible interface between the electrode and electrolyte, and allow the large storage of gravimetric capacitance, power and energy density. Unfortunately, the volumetric metrics in both capacitance and energy density (per volume of the active material) are not impressive due to their low packing densities [24,25].

Simultaneously achieving high areal and volumetric capacitances of MSCs remains a great challenge [1,26], because both of them tend to vary oppositely with the increased thickness of electrode films, in particular, composed of high surface area nanocarbon materials. For instance, electrochemically deposited films of onion-like carbon (OLC), with a specific surface area of 500 m^2/g, for MSCs was able to cycle at a high scan rate of 200 V/s,

* Corresponding authors.
E-mail addresses: xinliang.feng@tu-dresden.de (X. Feng), muellen@mpip-mainz.mpg.de (K. Müllen).

http://dx.doi.org/10.1016/j.ensm.2015.09.004
2405-8297/

but showed a low volumetric capacitance of 1.3 F/cm^3 [16]. Recently, a 7.6 μm-thick film of laser-scribed graphene, with exceptionally high surface area of over 1500 m^2/g, for MSCs demonstrated a high power density of 200 W/cm^3; however, the volumetric capacitance reported was only 3.05 F/cm^3 [27]. Similarly, other nanocarbon films consisting of high surface area NPC [19], reduced graphene oxide/CNTs (rGO/CNT) [28], vertically aligned CNTs (VACNT) [29] exhibited impressive areal capacitance of >5 mF/cm^2, but in most cases presented relatively low volumetric capacitance of <28 F/cm^3 due to their low packing densities (typically <0.5 g/cm^3). Undoubtedly, the low volumetric capacitance of these nanocarbon-based films for MSCs is attributed to the lack of advanced manufacture technologies that efficiently process high surface area activated materials into high packing density films. Currently, great efforts have been devoted to introducing new nanocarbon materials for MSCs, however, the reasonable design and manufacture of electrically conductive, highly porous, densely compact, binder- and additive- free films composed of high surface area nanocarbons have not been reported for high areal and volumetric capacitance MSCs.

In this work, we demonstrated the construction of binder-free, electrically conductive, highly porous, activated graphene (AG) compact films with remarkable areal capacitance and volumetric capacitance for high-performance MSCs. The binder-free AG compact films were fabricated by alternating deposition of two different graphene materials, e.g., electrochemically exfoliated graphene (EG) and nanoporous AG with a high specific surface area of 2920 m^2/g (Fig. 1a–e), and then dry transferring onto the target substrates (e.g., Si wafer) with a high-pressure mechanical densification process (Fig. 1f and g). Afterwards, the resulting compressed AG films exhibited uniform morphology in lateral dimensions, high conductivity (60 S/cm), nanoporous feature (<10 nm), and high packing density (0.65–0.8 g/cm^3). The all-solid-state planar MSCs (AG-MSCs) manufactured by lithographical micropatterns of the as-produced AG films on silicon wafers (Fig. 1h and i), delivered an unprecedented areal capacitance of 89.5 mF/cm^2 and volumetric capacitance of 147 F/cm^3 for MSCs. Moreover, the fabricated AG-MSCs could be operated at a large scan rate of 10,000 mV/s with a significant capacitance of 19.4 F/cm^3, and showed excellent long-life cycling stability (99.6% after 10,000 cycles).

2. Experimental

2.1. Synthesis of AG

The AG was fabricated by the KOH activation of graphene oxide (GO) derived from natural graphite flake by a modified Hummers method [30,31]. Typically, 50 mL GO with a high concentration of 7 mg/mL and 2100 mg KOH powder (mass ratio of GO:KOH is 1:6) were first dispersed into 50 mL water and strongly stirred for 1 h at a speed of 300 rpm. Then, the water in the mixed solution was naturally evaporated at 100 °C until black slurry of GO/KOH was formed. Afterward, the mixed slurry was directly transferred into a stainless steel tube and put into a furnace, and kept for 30 min in a N_2 gas flow of 300 ml/min, and heated at 110 °C for 1 h to dry the slurry. Further, the activation of GO was conducted at 700 °C for 1 h with a heating rate of 3 °C/min. After cooling down, the mixture was washed with 1 mol/L HCl to completely remove

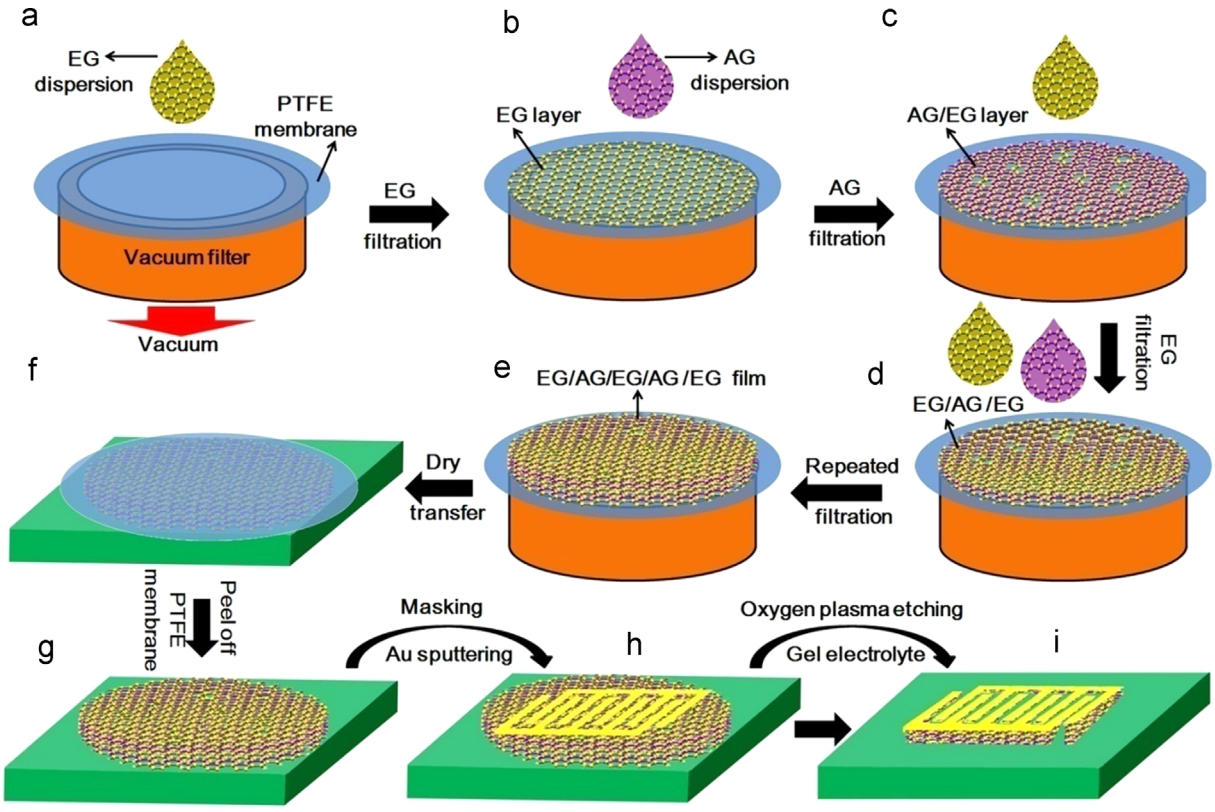

Fig. 1. Schematic illustration of binder-free AG compact films for in-plane MSCs. (a) Vacuum filtration of EG dispersion on a PTFE membrane filter. (b) Vacuum filtration of AG dispersion on the top of EG film. (c) Vacuum filtration of EG dispersion on the top of an AG/EG film. (d) Repeated filtration of the AG layer and EG layer on the EG/AG/EG film. (e) Dry transfer of the alternating deposited AG film (EG/AG/EG/AG/EG) on the surface of SiO_2/Si wafer under high pressure. (f) A compressed AG film on SiO_2/Si wafer after peeling off the PTFE membrane. (g) Thermally evaporation of gold micropatterns as current collector. (h) Oxygen plasma etching and drop-casting of gel electrolyte on interdigital electrodes. (i) An all-solid-state AG-MSC achieved.

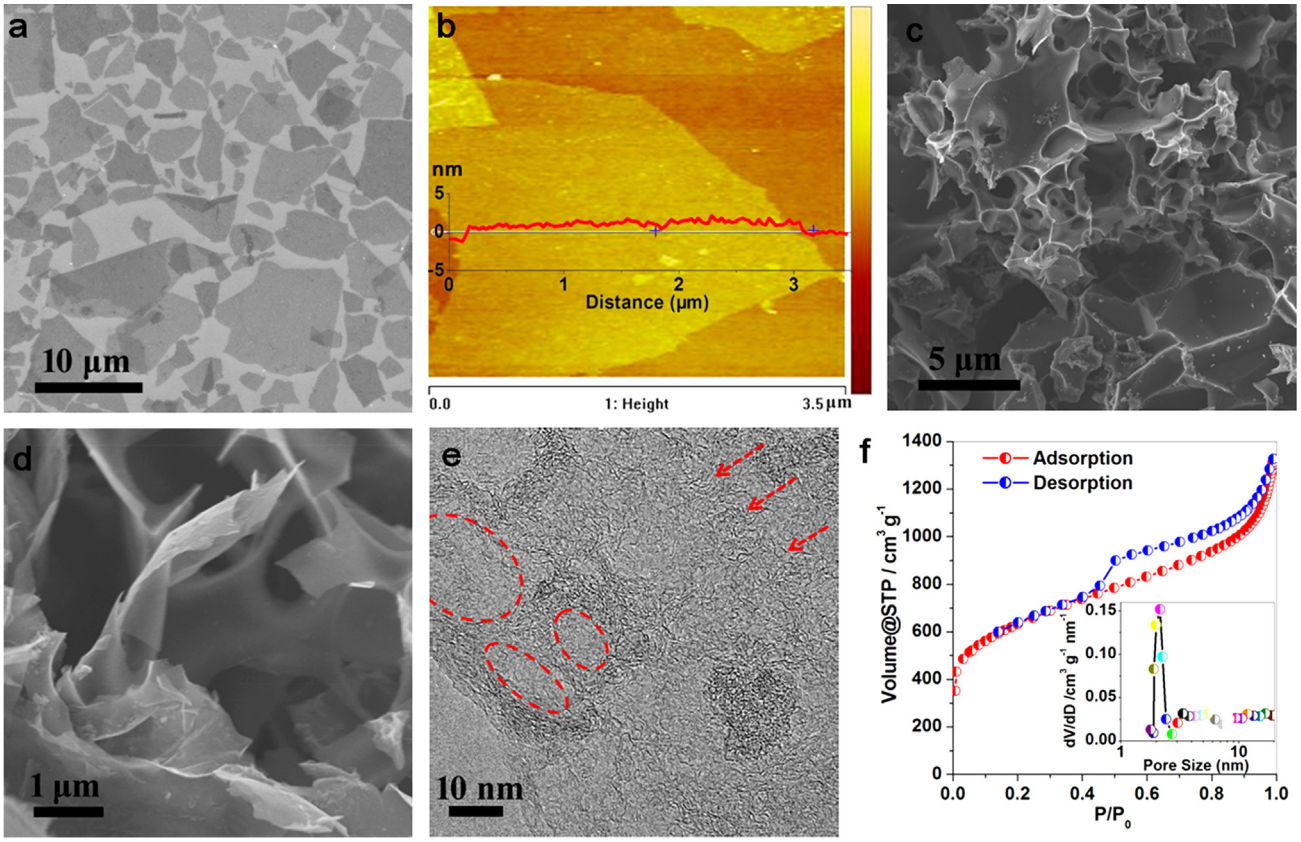

Fig. 2. (a) Low-magnification SEM image, and (b) AFM image (Inset: height profile) of EG nanosheets, showing the size of up to 10 μm, and a uniform flat thickness of less than 1.5 nm. (c) Low magnification SEM image of the AG. (d) High-magnification SEM image of the AG, showing the nature of thin edge in AG. (e) High-resolution TEM image of the AG, demonstrating the presence of micropore (indicated by arrows) and mesopore (indicated by red circles). (e) Isotherm plot and BJH pore distribution (inset) of AG confirm a high BET surface area (2920 $m^2\ g^{-1}$) and narrow nanopore size distribution (2.6 nm). (For interpretation of the references to color in this figure legend, the reader is referred to the web version of this article.)

residual KOH in ambient condition. The resulting AG powder was collected by simply filtering the above solution through a polytetrafluoroethylene (PTFE) membrane filter (pore size=0.2 μm, 47 mm in size), followed by water washing for three times. Finally, the AG powder was obtained after drying at 90 °C overnight.

2.2. Fabrication of the AG films

Electrochemically EG nanosheets were prepared according to our previous work [32,33]. 0.5 mg/mL of AG dispersed in N,N-Dimethylformamide (DMF) and 0.1 mg/mL EG dispersion in DMF were sonicated for at least 30 min. To fabricate the alternating stacked film, 5 mL EG dispersion was firstly filtrated to form the first bottom EG layer on the PTFE membrane. Afterwards, a controlled volume (e.g., 1, 3, 5 mL) of AG solution was immediately deposited on the top of the EG layer. Then, the same volume of EG dispersion was continuously added and filtered to obtain the second EG layer on the top of the AG/EG layer. Subsequently, AG layer and EG layer with the same volume and concentration were alternating deposited in sequence to form the AG films. Afterwards, the as-filtered AG film on PTFE membrane sandwiched by two pieces of PTFE plates was directly dry-transferred on the SiO_2/Si wafer with this home-made mechanical densification equipment (See the equipment in Fig. S1) overnight. Note that the pressure was applied until we could not rotate the top rotating handle by hand. Finally, the PTFE membrane was carefully peeled off to form a highly continuous AG film on Si wafer.

2.3. Fabrication of AG-MSCs

To fabricate AG-MSCs, 30 nm gold (99.9985% metals basis, Alfa Aesar) was thermally evaporated (EDWARDS FL400) on the AG film with a rate of ~1.0 Å s^{-1} and a chamber pressure of ~1×10^{-6} Torr using a home-made mask (widths of 210 μm, interspaces of 70 μm). Then, the microelectrode patterns of AG film on the SiO_2/Si wafer were created by oxidative etching of the exposed AG film in an O_2-plasma cleaner with 20 sccm O_2 flow for several minutes and 100~200 W rf power (Plasma System 200-G, Technics Plamsa GmbH). After that, a polymer gel electrolyte of PVA/H_2SO_4 was carefully drop-casted onto the surface of microelectrodes and solidified overnight. Finally, AG-MSCs with in-plane geometry were obtained. The gel electrolyte was prepared by mixing 6 g PVA (molecular weight 89,000–98,000, Sigma-Aldrich) and 6 g H_2SO_4 in 60 ml water, and heated at 85 °C for 1 h under stirring.

2.4. Materials characterization

The morphological and structural characterizations of samples were performed by scanning electron microscopy (SEM, Gemini 1530 LEO), transmission electron microscopy (TEM, FEI Tecnai T20 G^2, 200 kV), optical microscopy, atomic force microscopy (AFM, Veeco Dimension 3100), surface profiler (KLA Tencor P−16+), nitrogen adsorption and desorption and pore-size analysis at 77 K (Micromeritcs Tristar 3020 analyzer). The electrical conductivity of the films was measured by a standard four-point probe system with a Kiethley 2700 Multimeter.

2.5. Electrochemical characterization

Cyclic voltammerty (CV) measured at the different scan rates ranging from 1 mV/s to 10,000 mV s^{-1}, and electrochemical impedance spectroscopy (EIS) recorded in the frequency range of 0.01–100 kHz with a 5 mV ac amplitude was carried out by a CHI 760D electrochemical workstation. The detailed calculation of the areal capacitance, volumetric capacitance, energy density and power density is given in Supplementary material.

3. Results and discussion

The fabrication process of AG-MSCs is schematically illustrated in Fig. 1 (See details in Supplementary material). The binder-free compact film was firstly manufactured by alternating deposition of high-quality electrochemically exfoliated graphene (EG) nanosheets (Fig. 2a and b and Fig. S2) and high surface area nanoporous AG dispersion in sequence (Fig. 1a–e). Note that both the bottom layer and top layer of the films are the thin EG layers with a thickness of 20 nm (Fig. 1d and e), and the thickness of the AG layer as major component are fixed in micrometer scale. Then, the fabricated film was directly dry transferred onto the target Si wafer by a high-pressure mechanical densification process (Fig.1f). It should be emphasized that this mechanically compress process

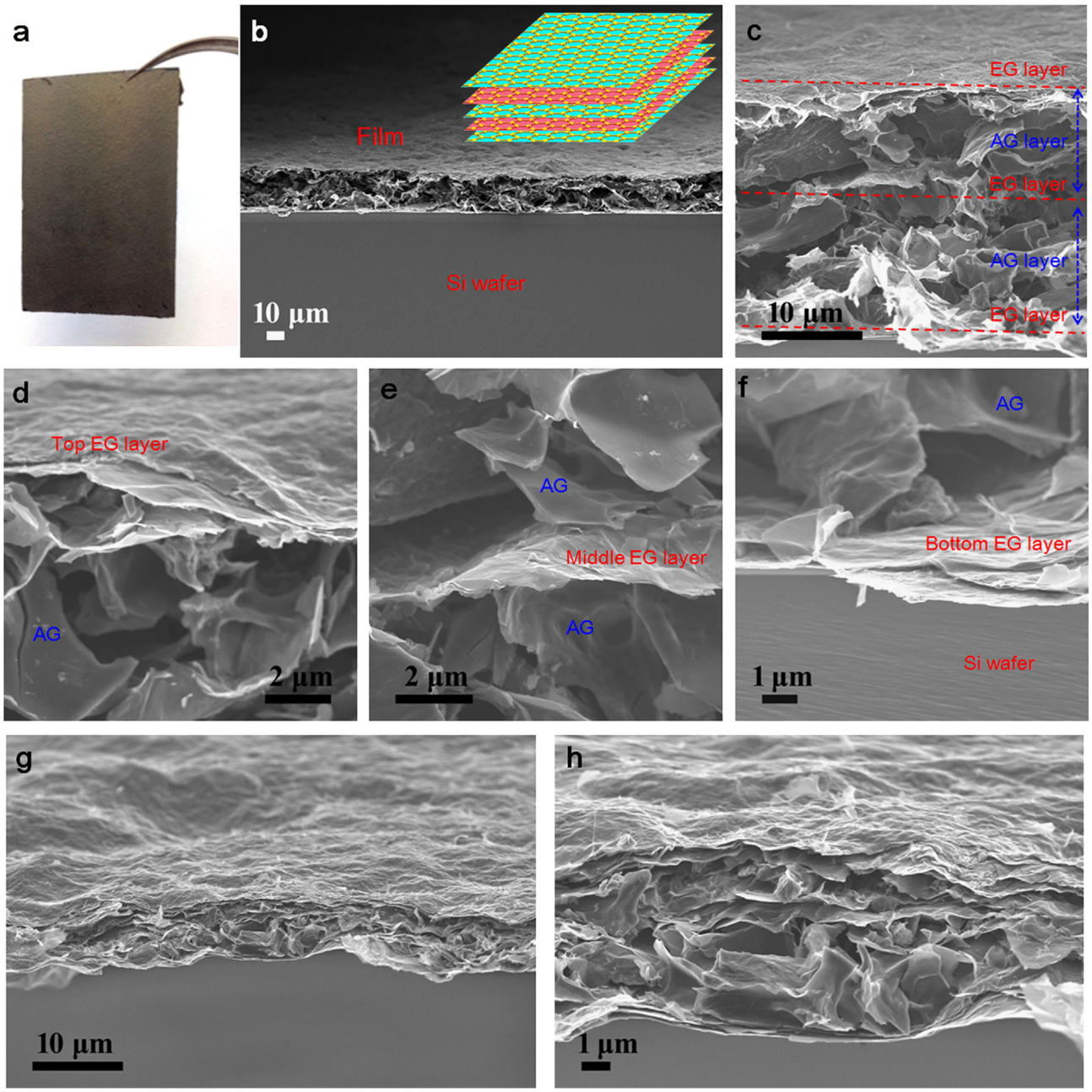

Fig. 3. (a) Optical image of the AG films transferred on SiO_2/Si wafer. (b) Low-magnification SEM images of AG films with a layer-by-layer stacked structure (as indicated by inset), showing the uniform thickness and compact structure. (c) High-magnification of the AG films with an alternating stacked structure consisting of EG layer and AG layer. (d) The top, (e) middle, and (f) bottom view of SEM images of AG films, showing the tightly stacked structure of the EG and AG layers. (g, h) Cross-section SEM image of a compact AG film with a densely layer-stacked structure.

is of great importance to overcome the low density of high surface area AG electrodes [34], which is responsible for the achievement of final high volumetric capacitance (See below). After peeling off the filtration membrane, a highly compact AG film was obtained on silicon wafer (Fig. 1g). Afterwards, the interdigital micro-electrodes of the AG films were patterned by thermal evaporation of Au layer with a customized mask (Fig. 1h) and subsequently treated with oxygen plasma etching (Fig. 1i, Fig. S3). Finally, after drop casting and solidification of a polymer gel electrolyte of polyvinyl alcohol/H_2SO_4 (PVA/H_2SO_4) on the project area of the device, an all-solid-state in-plane AG-MSC was fabricated (Fig. 1i).

The AG material was prepared using KOH chemical activation of GO, followed by thermal annealing at 700 °C for 1 h, and by neutralizing KOH with HCl. The nanopores and high surface area of AG were disclosed in Fig. 2c–f and Fig. S4. The low-magnification scanning electron microscopy (SEM, Fig. 2d, and Fig. S4a and b) and transmission electron microscopy (TEM, Fig. S4c) images show the typical morphologies of AG with a nanoporous structure, composed of ultrathin nanosheets as identified by the exposed edges of the stacked AG powder (Fig. 2d). High-resolution TEM (HRTEM) image (Fig. 2e, Fig. S4d) of AG further disclosed the highly curved, predominantly atom-thick sp^2-bonded carbon walls that present numerous nanopores of 1–10 nm in size. The extremely high specific surface area of up to 2920 m^2/g and narrow porous size distribution (average size of 2.6 nm) of AG materials were further confirmed by nitrogen adsorption and desorption measurement and pore size analysis (Fig. 2f), which are consistent with SEM and HRTEM characterizations. Therefore, these unique characteristics of AG can guarantee numerous available nanospaces for the fast accessibility of electrolyte ions during the electrochemical process [35].

To overcome the intractable issue of low packing density (0.36 g/cm^3) and volumetric capacitance (60 F/cm^3) of AG for supercapacitors [35,36], we developed the technique of alternating deposition with high-pressure dry transfer process to fabricate layer-stacked, high packing density, binder-free carbon films. Fig. 3 shows the morphology and microstructure of the as-prepared AG films alternatively deposited with three EG layers and two AG layers. Fig. 3a represents a completely transferred AG film covered on silicon wafer (a size of 3×2 cm^2), exhibiting a large area yet highly continuous film. Low-magnification SEM images unravel the formation of uniform thickness and flat structure in the films (Fig. 3b and Fig. S5), and good contact of the film with the underlying Si wafer. Cross-section SEM images of a 20-μm-thick film (Fig. 3c) showed a typical layer-stacked structure, constructed by three EG layers in nanometer thickness and two AG layers in micrometer thickness (Fig. 1d–f). Notably, the thickness of the films can be readily controlled from 2 to 20 μm by varying the deposited volume of the AG dispersion (Fig. S6) and the number of alternating deposition sequence. It should be emphasized that the top, middle and bottom layers (Fig. 3d–f) of the thin EG layers with a thickness of 20–50 nm, act as "an elastic and flexible network" that can significantly confine the loose AG powder into the continuous and densely packed films. Clearly, micro-meter sized AG particles can be well encapsulated by the adjacent EG layers with a densely layer-stacked structure (Fig. 3g and h). Furthermore, the

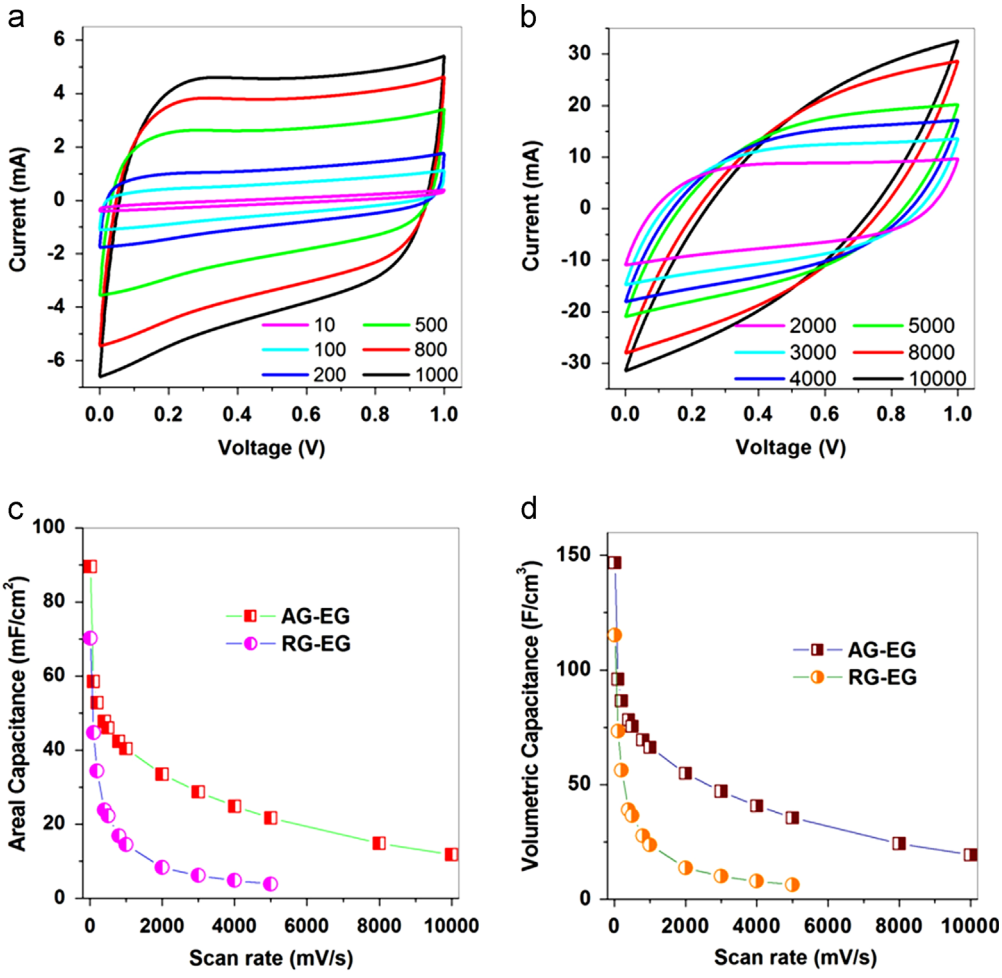

Fig. 4. (a, b) CV curves of AG-MSCs obtained at different scan rates, (a) from 10 to 1000 mV/s, and (b) from 2000 to 10,000 mV/s. (c) Areal capacitance and (d) volumetric capacitance for AG-MSCs and RG-MSCs.

resulting AG films (4 μm thick) presented a high electrical conductivity of 60 S/cm, due to the co-operative effect of layer-stacked EG and AG layers. Importantly, the continuous AG film has a high packing mass density, e.g., ranging from 0.65 to 0.8 g/cm^3 when the AG content in the films, in comparison with the AG powder (typically, 0.36 g/cm^3) [35], was increased properly from 40% to 80% (Fig. S7), suggestive of highly compact nature.

To evaluate the electrochemical properties of AG-MSCs, we first carried out cyclic voltammetry (CV) measurement at scan rates of from 10 to 10,000 mV s^{-1} (Fig. 4a and b). It was observed that AG-MSCs exhibited a typical double-layer capacitive featuring with a nearly rectangular CV shape in the scan rate range from 10 to 1000 mV/s (Fig. 4a), and maintained an impressive electrochemically charge storage at high charge and discharge of 10,000 mV s^{-1} (Fig. 4b). Remarkably, a linear dependence of the discharge current vs. the scan rate was recorded up to 2000 mV s^{-1} (Fig. S8), indicative of a high instantaneous power capability.

To further highlight the superiority of high specific surface area of AG for the performance enhancement of AG-MSCs, we fabricated in-plane MSCs (denoted as RG-MSCs) based on the alternating stacked film of low surface area reduced graphene oxide (RG) and EG, while keeping the mass loading of the film and cell assembly the same as for AG-MSCs. Noted that the RG powder in our previous work [37,38] presented a relatively low specific surface area of 190 m^2/g (Fig. S9), and seriously aggregated yet stacked morphology [38]. Nevertheless, the fabricated RG film with aid of thin EG layer showed the similar layer-stacked morphology to AG film, accompanied with highly uniformity and continuity (Fig. S10). The CV curves of RG-MSCs were examined at the scan rates ranging from 10 to 5000 mV/s (Fig. S11). The areal capacitance and volumetric capacitance for AG-MSCs and RG-MSCs were compared in Fig. 3c and d. Remarkably, the areal capacitance and volumetric capacitance of the AG-MSCs reached ~89.5 mF cm^{-2} and ~147 F cm^{-3}, respectively, both of which were superior to those of RG-MSCs (~70.3 mF cm^{-2} and ~115 F cm^{-3}; Fig. 4a and b), and the most reported carbon-based MSCs (Fig. S12), making them more competitive for prospective applications of miniaturized energy storage devices. Furthermore, it was disclosed that AG-MSCs exhibited much better rate capability than that of RG-MSCs. The areal and volumetric capacitances of the AG-MSCs dropped very slowly upon increasing the scan rates. For instance, areal capacitance of 40.4 mF cm^{-2} and volumetric capacitance of ~66.3 F cm^{-3} of AG-MSCs were maintained at a fast rate of 1000 mV/s, which are two times higher than those of RG-MSCs (14.5 mF cm^{-2} and ~23.8 F cm^{-3}). In particular, AG-MSCs even at 10,000 mV s^{-1} still delivered a significant areal capacitance of 11.8 mF cm^{-2} and volumetric capacitance of 19.4 F cm^{-3}. In contrast, RG-MSCs could not function at such high rate. The superior performance of AG-MSCs over RG-MSCs is intrinsically attributed to high specific surface area and nanoporous structure of AG powder.

To examine the fundamental behavior of MSCs, electrochemical impedance spectra (EIS) of AG-MSCs and RG-MSCs were measured in the frequency range from 0.1 Hz to 100 kHz at an open circuit voltage with an ac perturbation of 5 mV (Fig. 5a). The complex plane plot of AG-MSCs showed a more closed 90° slope than RG-MSCs,

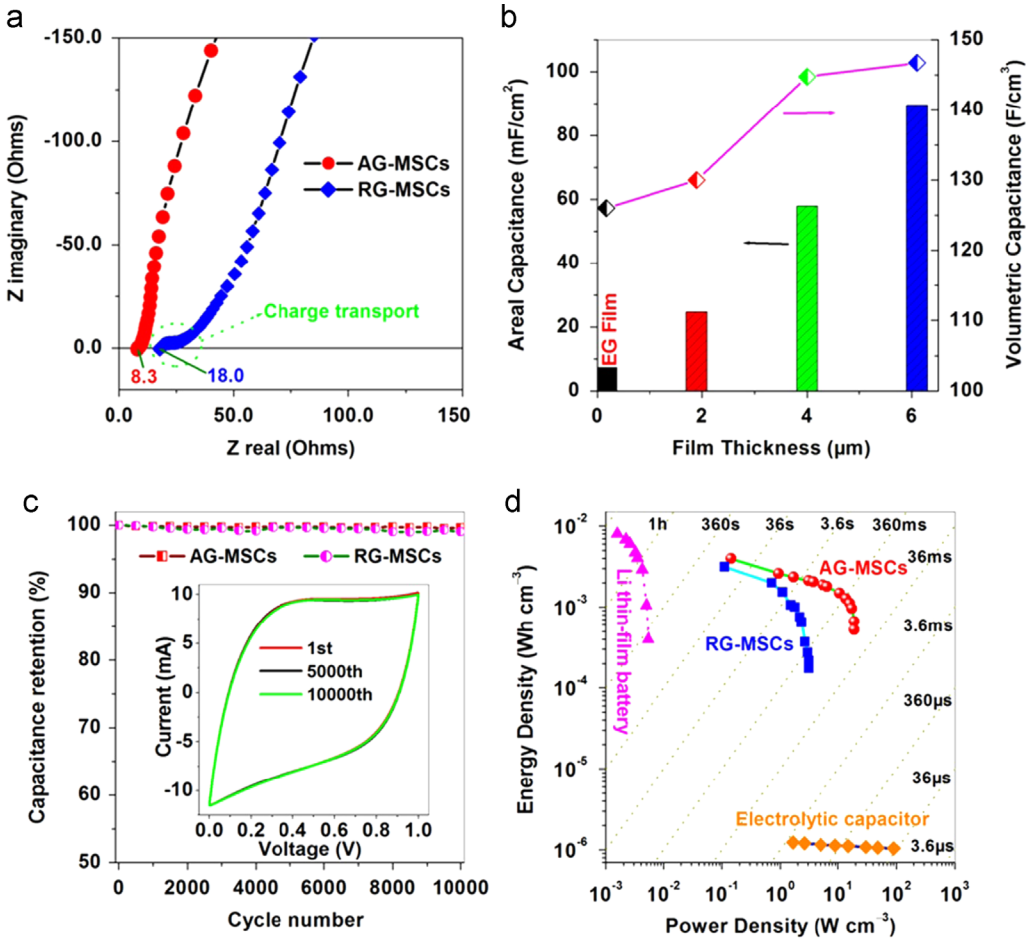

Fig. 5. (a) Electrochemical impedance spectroscopy of AG-MSCs and RG-MSCs. (b) Areal capacitance and volumetric capacitance of AG-MSCs as a function of the thickness of the AG films. (c) Cycling stability of AG-MSCs and RG-MSCs. Inset is the 1st, 5,000th, and 10,000th CV curves of AG-MSCs measured at 2000 mV s^{-1}. (d) Ragone plot of AG-MSCs, RG-MSCs, lithium thin-film battery (4 V/500 μA h) and electrolytic capacitor (3 V/300 μF).

indicative of a better capacitive characteristic of AG-MSCs. At high frequency region, AG-MSCs exhibited a lower equivalent series resistance (ESR) of 8.2 Ω than RG-MSCs (18.0 Ω), taken from the intercept at real part. It is known that the ESR represents a combined resistance of both electrical resistance of the electrodes and ion diffusion resistance inside the electrodes. Therefore, the lower ESR value of AG-MSCs highlights the superiority of AG film with high conductivity and micro-/meso-porous structure over RG film for high-rate MSCs. Another major difference is a visible small semicircle of RG-MSCs followed by a short 45° Warburg region appearing at high-frequency range, corresponding to the charge-transfer resistance of 12 Ω. Notably, this semicircle is not observable from AG-MSCs, suggesting the shortened ion diffusion pathway and low resistance from the external electrolyte to the interior surfaces.

The electrochemically cycling stabilities of AG-MSCs and RG-MSCs were further investigated for 10,000 cycles at a scan rate of 2000 mV s^{-1} (Fig. 5c). The CV shapes of AG-MSCs kept almost unchanged at different cycles (inset of Fig. 5c), indicative of outstanding electrochemical stability. Remarkably, it was evaluated that ~99.6% of the initial capacitance was maintained for AG-MSCs, which is better than that of RG-MSCs with retention of ~99.0% after 10,000 cycles (Fig. 5c).

The Ragone plot shown in Fig. 5d was further employed to compare the volumetric energy density and power density of AG-MSCs and RG-MSCs. It was revealed that the maximum volumetric energy density of AG-MSCs obtained at a discharge time of 100 s was 4.0 mW h/cm^3, which is higher than that of RG-MSCs (3.1 mW h/cm^3), and superior to most reported high surface area nanocarbon-based MSCs (Fig. S13), e.g., VACNT (0.3 mW h/cm^3) [29], rGO/CNT (0.68 mW h/cm^3) [28], NPC (1.9 mW h/cm^3) [19], laser written graphene oxide film (0.43 mW h/cm^3) [20], onion-like carbon (1.6 mW h/cm^3) [16], laser scribed graphene film (2.0 mW h/cm^3) [27], methane plasma reduced graphene (2.5 mW h/cm^3) [3], inkjet-printed carbon (2.3 mW h/cm^3) [13], and carbide-derived carbon (3.2 mW h/cm^3) [39]. Further, AG-MSCs exhibited a high power density of 18.9 W/cm^3, accompanied with an impressive energy density of 0.52 mW h/cm^3 achieved at a short discharge time of only 0.1 s. In sharp contrast, the RG-MSCs showed a fast degradation of energy density with increased high power density, e.g., a maximum power density with a low value of 3.1 W/cm^3 at 0.17 mW h/cm^3.

The excellent performance of AG-MSCs are substantially attributable to the reasonable utilization of the advantages of two type different graphene based materials (AG and EG) and efficient manufacture technique of processing the compact binder-free film [26]. Firstly, the AG with high specific surface area and micro/meso-porous structure can guarantee high double layer capacitance and excellent cycling stability. Secondly, the thin EG layer not only offers the elastically spatial confinement effect for the adjacent AG layers to promote the formation of the continuous films, but also acts as electrically conductive backbone pathway for rapid electron transport as well as capacitive contribution. Thirdly, the resulting films are high conductivity, nanoporous and compact structure, yet without added polymer binder and conductive additives, which can synergistically ensure rapid ion diffusion and electron transport [34,40], leading to high volumetric capacitance, energy and power densities [14,39].

4. Conclusion

In summary, we demonstrated the fabrication of binder-free EG-assisted AG compact films with exceptionally high areal capacitance and volumetric capacitance for high-performance MSCs, associated with excellent rate capability and cycling stability. This new densely layer-packed film endowed fast ion diffusion and electron transport throughout the binder-free film electrode, which would open up numerous opportunities for the promising applications, e.g., high- volumetric supercapacitors, lithium ion batteries, sensors, actuators, gas storage.

Acknowledgments

This work was financially supported by the ERC Grant on 2DMATER and NANOGRAPH, DFG SPP 1459, BMBF INSOCELL and EC under Graphene Flagship (No. CNECT-ICT-604391).

Appendix A. Supplementary material

Supplementary data associated with this article can be found in the online version at http://dx.doi.org/10.1016/j.ensm.2015.09.004.

References

[1] Z.S. Wu, X.L. Feng, H.M. Cheng, Recent advances in graphene-based planar micro-supercapacitors for on-chip energy storage, Natl. Sci. Rev. 1 (2014) 277–292.
[2] M.F. El-Kady, R.B. Kaner, Scalable fabrication of high-power graphene micro-supercapacitors for flexible and on-chip energy storage, Nat. Commun. 4 (2013) 1475.
[3] Z.S. Wu, K. Parvez, X.L. Feng, K. Müllen., Graphene-based in-plane micro-supercapacitors with high power and energy densities, Nat. Commun. 4 (2013) 2487.
[4] M. Beidaghi, Y. Gogotsi, Capacitive energy storage in micro-scale devices: recent advances in design and fabrication of micro-supercapacitors, Energy Environ. Sci. 7 (2014) 867–884.
[5] S. Makino, Y. Yamauchi, W. Sugimoto, Synthesis of electro-deposited ordered mesoporous RuO_x using lyotropic liquid crystal and application toward micro-supercapacitors, J. Power Sources 227 (2013) 153–160.
[6] M.Q. Xue, Z. Xie, L.S. Zhang, X.L. Ma, X.L. Wu, Y.G. Guo, W.G. Song, Z.B. Li, T.B. Cao., Microfluidic etching for fabrication of flexible and all-solid-state micro supercapacitor based on MnO_2 nanoparticles, Nanoscale 3 (2011) 2703–2708.
[7] J. Feng, X. Sun, C.Z. Wu, L.L. Peng, C.W. Lin, S.L. Hu, J.L. Yang, Y. Xie, Metallic few-layered VS_2 ultrathin nanosheets: High two-dimensional conductivity for in-plane supercapacitors, J. Am. Chem. Soc. 133 (2011) 17832–17838.
[8] J.H. Sung, S.J. Kim, K.H. Lee, Fabrication of microcapacitors using conducting polymer microelectrodes, J. Power Sources 124 (2003) 343–350.
[9] W.W. Liu, X.B. Yan, J.T. Chen, Y.Q. Feng, Q.J. Xue., Novel and high-performance asymmetric micro-supercapacitors based on graphene quantum dots and polyaniline nanofibers, Nanoscale 5 (2013) 6053–6062.
[10] C. Meng, J. Maeng, S.W.M. John, P.P. Irazoqui., Ultrasmall integrated 3D micro-supercapacitors solve energy storage for miniature devices, Adv. Energy Mater. 3 (2014) 1301269–1301275.
[11] X. Xiao, C. Zhang, S. Lin, L. Huang, Z. Hu, Y. Cheng, T. Li, W. Qiao, D. Long, Y. Huang, L. Mai, Y. Gogotsi, J. Zhou, Intercalation of cations into partially reduced molybdenum oxide for high-rate pseudocapacitors, Energy Storage Mater. 1 (2015) 1–8.
[12] H. Durou, D. Pech, D. Colin, P. Simon, P.L. Taberna, M. Brunet, Wafer-level fabrication process for fully encapsulated micro-supercapacitors with high specific energy, Microsyst. Technol. 18 (2012) 467–473.
[13] D. Pech, M. Brunet, P.L. Taberna, P. Simon, N. Fabre, F. Mesnilgrente, V. Conedera, H. Durou, Elaboration of a microstructured inkjet-printed carbon electrochemical capacitor, J. Power Sources 195 (2010) 1266–1269.
[14] J. Chmiola, C. Largeot, P.L. Taberna, P. Simon, Y. Gogotsi, Monolithic carbide-derived carbon films for micro-supercapacitors, Science 328 (2010) 480–483.
[15] P. Huang, M. Heon, D. Pech, M. Brunet, P.L. Taberna, Y. Gogotsi, S. Lofland, J. D. Hettinger, P. Simon, Micro-supercapacitors from carbide derived carbon (CDC) films on silicon chips, J. Power Sources 225 (2013) 240–244.
[16] D. Pech, M. Brunet, H. Durou, P.H. Huang, V. Mochalin, Y. Gogotsi, P.L. Taberna, P. Simon, Ultrahigh-power micrometre-sized supercapacitors based on onion-like carbon, Nat. Nanotechnol. 5 (2010) 651–654.
[17] H.J. Ahn, W.B. Kim, T.Y. Seong., $Co(OH)_2$-combined carbon-nanotube array electrodes for high-performance micro-electrochemical capacitors, Electrochem. Commun. 10 (2008) 1284–1287.
[18] D. Kim, G. Shin, Y.J. Kang, W. Kim, J.S. Ha, Fabrication of a stretchable solid-state micro-supercapacitor array, ACS Nano 7 (2013) 7975–7982.
[19] C.W. Shen, X.H. Wang, W.F. Zhang, F.Y. Kang, Direct prototyping of patterned nanoporous carbon: A route from materials to on-chip devices, Sci. Rep. 3 (2013) 2294.
[20] W. Gao, N. Singh, L. Song, Z. Liu, A.L.M. Reddy, L.J. Ci, R. Vajtai, Q. Zhang, B.Q. Wei, P.M. Ajayan, Direct laser writing of micro-supercapacitors on hydrated graphite oxide films, Nat. Nanotechnol. 6 (2011) 496–500.

[21] J.J. Yoo, K. Balakrishnan, J.S. Huang, V. Meunier, B.G. Sumpter, A. Srivastava, M. Conway, A.L.M. Reddy, J. Yu, R. Vajtai, P.M. Ajayan, Ultrathin planar graphene supercapacitors, Nano Lett. 11 (2011) 1423–1427.
[22] Z.Q. Niu, L. Zhang, L.L. Liu, B.W. Zhu, H.B. Dong, X.D. Chen, All-solid-state flexible ultrathin micro-supercapacitors based on graphene, Adv. Mater. 25 (2013) 4035–4042.
[23] W.W. Liu, Y.Q. Feng, X.B. Yan, J.T. Chen, Q.J. Xue, Superior micro-supercapacitors based on graphene quantum dots, Adv. Funct. Mater. 23 (2013) 4111–4122.
[24] Y.P. Zhai, Y.Q. Dou, D.Y. Zhao, P.F. Fulvio, R.T. Mayes, S. Dai, Carbon materials for chemical capacitive energy storage, Adv. Mater. 23 (2011) 4828–4850.
[25] C. Liu, F. Li, L.P. Ma, H.M. Cheng, Advanced materials for energy storage, Adv. Mater. 22 (2010) E28–E62.
[26] Z.S. Wu, K. Parvez, S. Li, S. Yang, Z. Liu, S. Liu, X. Feng, K. Müllen, Alternating stacked graphene-conducting polymer compact films with ultra high areal and volumetric capacitances for high-energy micro-supercapacitors, Adv. Mater.
[27] M.F. El-Kady, R.B. Kaner, Scalable fabrication of high-power graphene micro-supercapacitors for flexible and on-chip energy storage, Nat. Commun. 4 (2013) 1475.
[28] M. Beidaghi, C.L. Wang, Micro-supercapacitors based on interdigital electrodes of reduced graphene oxide and carbon nanotube composites with ultra high power handling performance, Adv. Funct. Mater. 22 (2012) 4501–4510.
[29] A. Ghosh, V.T. Le, J.J. Bae, Y.H. Lee, TLM-PSD model for optimization of energy and power density of vertically aligned carbon nanotube supercapacitor, Sci. Rep. 3 (2013) 2939.
[30] Z.S. Wu, A. Winter, L. Chen, Y. Sun, A. Turchanin, X. Feng, K. Müllen, Three-dimensional nitrogen and boron co-doped graphene for high-performance all-solid-state supercapacitors, Adv. Mater. 24 (2012) 5130–5135.
[31] Z.S. Wu, Y. Sun, Y.Z. Tan, S.B. Yang, X.L. Feng, K. Müllen, Three-dimensional graphene-based macro- and mesoporous frameworks for high-performance electrochemical capacitive energy storage, J. Am. Chem. Soc. 134 (2012) 19532–19535.
[32] K. Parvez, Z.S. Wu, R. Li, X. Liu, R. Graf, X. Feng, K. Müllen, Exfoliation of graphite into graphene in aqueous solutions of inorganic salts, J. Am. Chem. Soc. 136 (2014) 6083–6091.
[33] K. Parvez, R.J. Li, S.R. Puniredd, Y. Hernandez, F. Hinkel, S.H. Wang, X.L. Feng, K. Müllen, Electrochemically exfoliated graphene as solution-processable, highly conductive electrodes for organic electronics, ACS Nano 7 (2013) 3598–3606.
[34] S. Murali, N. Quarles, L.L. Zhang, J.R. Potts, Z.Q. Tan, Y.L. Lu, Y.W. Zhu, R.S. Ruoff, Volumetric capacitance of compressed activated microwave-expanded graphite oxide (a-MEGO) electrodes, Nano Energy 2 (2013) 764–768.
[35] Y.W. Zhu, S. Murali, M.D. Stoller, K.J. Ganesh, W.W. Cai, P.J. Ferreira, A. Pirkle, R.M. Wallace, K.A. Cychosz, M. Thommes, D. Su, E.A. Stach, R.S. Ruoff, Carbon-based supercapacitors produced by activation of graphene, Science 332 (2011) 1537–1541.
[36] W.Y. Tsai, R.Y. Lin, S. Murali, L.L. Zhang, J.K. McDonough, R.S. Ruoff, P.L. Taberna, Y. Gogotsi, P. Simon, Outstanding performance of activated graphene based supercapacitors in ionic liquid electrolyte from −50 to 80 degrees, Nano Energy 2 (2013) 403–411.
[37] Z.S. Wu, W. Ren, L. Gao, B. Liu, C. Jiang, H.M. Cheng, Synthesis of high-quality graphene with a pre-determined number of layers, Carbon 47 (2009) 493–499.
[38] Z.S. Wu, S.F. Pei, W.C. Ren, D.M. Tang, L.B. Gao, B.L. Liu, F. Li, C. Liu, H.M. Cheng, Field emission of single-layer graphene films prepared by electrophoretic deposition, Adv. Mater. 21 (2009) 1756–1760.
[39] M. Heon, S. Lofland, J. Applegate, R. Nolte, E. Cortes, J.D. Hettinger, P.L. Taberna, P. Simon, P.H. Huang, M. Brunet, Y. Gogotsi, Continuous carbide-derived carbon films with high volumetric capacitance, Energy Environ. Sci. 4 (2011) 135–138.
[40] M.R. Lukatskaya, O. Mashtalir, C.E. Ren, Y. Dall'Agnese, P. Rozier, P.L. Taberna, M. Naguib, P. Simon, M.W. Barsoum, Y. Gogotsi, Cation intercalation and high volumetric capacitance of two-dimensional titanium carbide, Science 341 (2013) 1502–1505.